SERSIO: Svalbard EISCAT Rocket Study of Ion Outflows

K. M. Frederick-Frost, K. A. Lynch
Department of Physics and Astronomy, Dartmouth College, Hanover, New Hampshire, USA

P. M. Kintner Jr.
Department of Electrical and Computer Engineering, Cornell University, Ithaca, New York, USA

E. Klatt
Applied Physics Laboratory, Johns Hopkins University, Laurel, Maryland, USA

D. Lorentzen, J. Moen
Department of Physics, University of Oslo, Oslo, Norway

Y. Ogawa
Solar-Terrestrial Environment Laboratory, Nagoya University, Nagoya, Japan

M. Widholm
Institute for the Study of Earth, Oceans and Space, University of New Hampshire, Durham, New Hamphire, USA

The SERSIO sounding rocket was launched from Ny-Alesund, Svalbard into an ion upflow event simultaneously observed by the EISCAT radar facility in Longyearbyen on January 22, 2004 at 0857 UT. It reached an apogee of 782 km. In situ wave data and thermal particle measurements in the cusp/cleft region clearly show core thermal ion temperature enhancements up to 0.8 eV in association with 0-4kHz broadband extremely low frequency wave activity (BBELF). The in situ observation of wave heating in the cusp/cleft region at these low altitudes (520-780 km) is a new measurement and should be included in any multi-stage model of ion energization. Wave activity in the form of naturally enhanced ion acoustic lines (NEIAL) was seen by the EISCAT radar in the same activity region. Periods of NEIAL were compared with in situ auroral electron data which show no evidence of a bump-on-tail distribution, thus our data do not support using Langmuir turbulence to explain these radar echoes. In contrast, these observations associating NEIAL with BBELF activity suggest that they may be the same phenomenon. In situ measurements also confirm the link between soft electron precipitation and thermal electron temperature enhancements in this ion upflow environment. Electron temperature enhancements can reduce instability thresholds for the current driven instabilities thought to drive BBELF activity.

1. INTRODUCTION

Much insight into the interaction between the Earth's magnetosphere and ionosphere can be obtained by study of the cusp/cleft region. Specifically, the processes leading to the energization of heavy ions in the ionosphere and subsequent escape to the magnetosphere have been the focus a great deal of observation and modeling [*Hultqvist et al.,* 1999]. It is recognized that the field aligned ion upflows seen by ground based radar are the seeds

of the outflowing cold O+, H+ population seen at satellite altitudes. Up/outflows therefore also provide an opportunity for radar and in situ communities to co-examine proposed ion energization mechanisms such as ambipolar electric fields due to increased electron scale height, frictional heating from convective flows, and perpendicular wave heating which can lead to mirror force driven outflow.

Incoherent scatter radars (ISR) observe field aligned ion flows increasing in velocity (up to 1500 m/s) with increasing altitude. *Wahlund et al.* [1992] identified two classes of upflows, one associated with large convective flows and another correlated with electron precipitation, located within aurorae. Radar observations of naturally enhanced ion acoustic lines, NEIAL, interpreted as the effects of wave activity, are often seen in conjunction with ion upflows [*Forme* 1995, *Ogawa et al.,*2000], but the exact form of the wave activity is unknown and not measurable by the radar. ISR interferometer experiments suggest that NEIALs occur in narrow regions, under 1 km transverse to the magnetic field [*Grydeland et al.,* 2005], at altitudes of several hundred km to the upper limit of ISR observability, about 800 km. Although most experiments have examined wave vectors parallel to the magnetic field, NEIAL are observed for wave vectors up to 15 degrees from parallel [*Collis et al*. 1991].

Proposed drivers for ion energization are also well studied at satellite altitudes. *Strangeway et al*. [2004] *and Zheng et al.* [2004] found in statistical surveys of FAST and POLAR satellite data respectively that outflowing ions were correlated with soft electron precipitation and to a slightly lesser degree, downward directed Poynting flux. The former finding is in agreement with *Seo et al.* [1997] who identified the anti-correlation of precipitating electron energy and ion upflux at low DE-2 satellite (850-950 km) altitudes. *Ogawa et al.* [2003] used DMSP and EISCAT to show soft precipitation primarily drives ion upflow. *Lynch et al.* [2002] showed a strong correlation between ion conics in downward current region aurora, and BBELF activity.

Combining ground and satellite perspectives, one can view up/outflows as a multistage process with low altitude heating or upwelling leading to scale height increase into regions of ELF wave activity and subsequent energization to escape velocities. Open questions involve what happens in between those altitudes and how low in altitude we can expect to see wave heating. What is the specific wave-particle interaction for the wave heating, and what is the driver (energy source) for it?

Rocket studies provide high resolution and localized in situ data at these 400-2000 km altitudes. The SCIFER sounding rocket [*Kintner et al.* 1996a, 1996b, and *Arnoldy* 1996] was launched from Andoya Rocket Range into the cusp/cleft region (at 1400 km) and provided evidence of ~30 km regions of transversely accelerated ions (TAI) in association with broadband extremely low frequency wave activity (BBELF). SCIFER HF data also indicated depletions of the ionospheric density in these localized regions of wave heating. To further investigate lower altitude signatures of ion heating in the cusp/cleft (~750 km), we report here on the Jan 22, 2004 flight of the SERSIO sounding rocket mission, which included thermal electron and ion instrumentation. A more

complete account of the ground-based data for the Jan 22, 2004 event is given in a paper by *Lorentzen et al.* [2006].

We will begin with an overview of the SERSIO experiment: its campaign goals, payload configuration, launch event and flight performance. This is followed by a presentation of all sky camera, EISCAT, and in situ particle and wave data for the event. Analysis of the auroral precipitation, thermal ions and electrons, and BBELF activity will show evidence of wave induced ion heating in the 520-780 km range. The observed relationship between soft precipitation and enhanced electron temperature supports the idea that the driver for BBELF is a current-driven instability. We also explore connections between BBELF and NEIAL activity, and describe the new ERPA instrument, first flown on this mission. The SERSIO flight provides a rare opportunity to examine the same event with both in situ and ground based radar data.

2. THE SERSIO EXPERIMENT

The Svalbard EISCAT Rocket Study of Ion Outflows (SERSIO) mission was designed to quantify the extent to which wave particle interactions, ambipolar electric fields, and joule heating assist in the upflow/outflow of cold heavy ions from the ionosphere. The payload contained three hemispherical electrostatic (top hat) analyzers [*Carlson et al.*, 1983, and *Young et al.,* 1988], which provided velocity distributions for electrons (5-16000 eV) and ions (200 – 8000 eV). Three additional top hat detectors covered the thermal ion population (0.1-20 eV), one of which provided O+, H+ mass separation [*Lynch*, 1999]. Thermal electrons were characterized by a retarding potential analyzer (ERPA) [see appendix] on the sub payload and a thermal electron detector (TED) (0.1-6eV) on the main payload. The top hat detectors and the TED [*MacDonald*, 2005 manuscript submitted] were placed on 1 m long booms to avoid effects of the payload sheath. Particle instrumentation on this NASA 35.035 flight was optimized to study the thermal core of the ionosphere, providing a touchstone for comparison with the EISCAT radars in Tromso and Longyearbyen which simultaneously provided bulk line-of-sight ionospheric parameters. In situ wave data were collected from the Cornell Wire Boom Yo-Yo System (COWBOY) [*Klatt,* 2005]. Ejected as a sub payload, the COWBOY was designed to deploy two twelve meter tip-to-tip sensors for detection of long wavelength plasma waves and DC electric fields.

SERSIO was launched into the cusp/cleft on a South-West trajectory from Ny-Alesund, Svalbard, Norway January 22, 2004 at 0857 UT, providing approximately 15 minutes of in situ data and obtaining an apogee of 782 km. At the time the ionosphere was responding to a strong pressure pulse from a coronal mass ejection. Roughly 10 min before launch the IMF Bz component rotated from south to north. For the flight, IMF Bz (approx 10 to 20 nT) was northward and By was approximately –20nT, making the ideal conditions for high-latitude reconnection. The solar wind speed was about 650 km/s and the density was variable, 7-20 /cc. During the SERSIO flight, all sky camera (ASC) observations showed pulsating 6300 Å [OI] emissions of a temporal origin. The pulsations lasted throughout the flight, with periods of 8-10 minutes. The 6300 Å [OI] emission intensities were high (> 10 kR), accompanied by less intense (~2 kR), more

localized, 5577 Å [OI] emissions (Figure 1). The launch was called from the UNIS facility in Longyearbyen during an extended period of ion upflow (Figure 2).

To ensure the main payload remained within 10 degrees of the earth's magnetic field, an attitude control system (ACS) was utilized. The ACS system did not work and the main payload settled into a flat spin roughly perpendicular to **B**. The booms did not fully deploy, and the sub payload was ejected with a coning half angle far in excess of success criteria. As a result, the final position of the detectors is only roughly known, and the COWBOY antennas unraveled in a fashion that effectively created two different baselines approximately 1.8m and 5.5m long. Thus DC **E** vectors, particle pitch angle, and wave **k** vector information are not available, although wave frequency information and particle energy were obtained. We are able to construct energy and temperature profiles of the ions and electrons and obtain 0-20kHz frequency information from the COWBOY. The intensity and duration of the event and its extensive ground coverage justify the use of even this somewhat limited in situ data set.

3. DATA HANDLING

3.1 Radar data

During the timeframe of the SERSIO flight, data were obtained by the ESR facility located in Longyearbyen, Svalbard. The EISCAT Svalbard radar operates at 500 MHz so that coherent observations are produced by 30 cm waves. The 42 m 500MHz dish is permanently directed along the magnetic field and provided plasma parameters along the magnetic field line. The 32 m dish was pointed to intersect the payload trajectory at 563 km on the upleg; at that point it made an 18 degree angle with the magnetic field. Ion and electron temperatures were derived from EISCAT data assuming Maxwellian distributions. Errors in the radar derived plasma parameters come from the difference between observed and fitted theoretical Incoherent Scatter (IS) spectra. NEIALs were identified between 500-1000 km when there was a peak in IS signals above the F2 peak. NEIALs were carefully distinguished from satellite echoes.

3.2 In situ particle data

To extract ion temperature data from the in situ electrostatic analyzers the following assumptions were made. Firstly, we assumed that the thermal ion distribution, f, was Maxwellian, allowing us to find a temperature from the slope of $\ln(f)$ vs. energy, E. Secondly the dominant majority of the ions detected lie in the ram/flow direction, allowing a simplification to that for one look direction. We used the observed low energy cut-off from the thermal ion spectra to estimate the payload potential (though this agrees quite well with an electron temperature calculation of the payload potential based on ERPA data). Lastly, because we do not know the exact attitude of the detector aperture plane with respect to the ram direction, we use the full ram vector in our calculation of the rammed Maxwellian, noting that we average our data over the payload spin. Within each spin, the 2D aperture is exposed to the full effect of payload ram velocity.

The effect of the payload's motion, or ram, is to shift each piece of the distribution $f(v_{Mx})$ by a velocity, v_R. The payload potential, Φ, adds to the energy of each particle. The effect is that the energy of each ion measured by the detector, $E(v)$, differs from the

Maxwellian value, $E_{Mx}(v_{Mx})$. Thus, we must correct our measured temperature, $T(v)$, to match the Maxwellian temperature, $T_{Mx}(v,\Box)$, in the following way.

$$E_{Mx} = \frac{1}{2} m v_{Mx}^2$$

$$E = \frac{1}{2} m v^2$$

$$\frac{1}{2} m v^2 = \frac{1}{2} m (v_{Mx} + v_R)^2 + e\Box$$

$$\frac{\Box \ln f}{\Box E_{Mx}} = \Box \frac{1}{T_{Mx}}$$

$$\frac{\Box \ln f}{\Box E} = \Box \frac{1}{T}$$

$$T_{Mx} = T \frac{\Box E_{Mx}}{\Box E}$$

It should be noted that any convective plasma flows should be accounted for in a similar manner as the ram velocity. Given the ACS failure, we do not have in situ DC electric field data. Thus, our ion temperatures err in that we can not properly account for flows; this ambiguity is considered in the Discussion section below. See Figure 3a for an example of a typical temperature fit. Adjusting the chosen fit start and end points gives a fit error of +/- 0.03 eV to our corrected temperatures. Typical count values range from 250-750 counts per spin average, giving approximately 6% Poisson noise. Higher energy electron data are negligibly affected by ram and spacecraft potential. Figure 3b shows an example of the log of the distribution of the auroral electrons versus energy at 423 s TOF.

In conjunction with the top hat thermal ion detectors, the ERPA retarding potential analyzer (described in Appendix) was used to obtain thermal electron temperatures by similarly assuming a Maxwellian distribution. Ram effects need not be considered due to the much higher thermal velocities of the electrons. Following the formalism above, without a ram velocity, the spacecraft potential simply produces an energy shift that drops out when calculating $\Box$E. Therefore the thermal electron temperature can be obtained from a simple line fit of the natural log of the electron spectra tail.

3.3 In situ field data

The subpayload carrying the COWBOY boom system was designed to deploy two 12 m flexible wire crossed dipoles with spherical sensors at the tips with the dipoles perpendicular to the local magnetic field (helicopter mode). The ACS failure drove the entire assembly unstable and it reached a final state about 60 s after the boom deployment. In the final state (Figure 4) the 4 wire booms extended roughly parallel along the symmetry axis of the subpayload taking on the appearance of a squid. Analysis of the signals yielded a robust geometry of the final state with the 1, 2, and 3 sensors collocated (the 1 and 2 sensors were in contact) and the 4 sensor about 1.8 meters away.

The booms were all roughly perpendicular to the magnetic field and 3-4 sensor separation was also roughly perpendicular to the magnetic field. The useable signals were the VLF channels (10 Hz to 20 kHz) from the subpayload skin to the 3 and 4 sensors with baselines of 5.5 m and 5.9 m respectively and the VLF channel on the 3-4 sensor combination with a baseline of 1.8 m. The 1.8 m baseline was close to perpendicular to the skin to sensors 3 and 4 baselines.

4. DATA PRESENTATION

4.1 Ground data

All sky camera images taken from Ny-Alesund during the SERSIO flight are shown in Figure 1. The camera is maintained/operated by the University of Oslo. The 6300 Å emissions shown here are projected to 250km altitude and are mapped over Svalbard. Figures 1a, 1b, 1c, are taken at 0901 UT, 0905 UT, and 0910 UT respectively. At these times, SERSIO is roughly at 500 km upleg, at apogee, and at 500 km downleg. The nominal trajectory is demarcated by yellow squares, whereas the 500 km up and downleg altitudes are red squares. The 32 m EISCAT beam is shown in white and the Tromso UHF beam in blue. The 42 m EISCAT beam looks straight up the field line. The star notes the position of the two radars. The 6300 Å emission intensifies near apogee and is seen over Longyearbyen during the time of the flight. At 563 km, the EISCAT 32 m beam intersects the nominal trajectory. After 0902 UT, this intersection altitude is not in the emission region.

Figure 2 shows a summary of the EISCAT 42 m data, and Figure 5a shows 249 second integrated line profiles obtained by the EISCAT 42 m dish between 8:58:40 - 9:02:49 UT (100 – 349 s TOF). These figures show the characteristics of the ion upflow event in which we acquired in situ data. Ion velocities in excess of 500 m/s were seen above 600 km and enhanced electron temperatures up to 6000 degrees K were recorded. EISCAT ion temperatures are typically less than 2000 degrees K for this event. Figure 5b shows SERSIO in situ thermal ion and electron temperatures in a similar format obtained between 0900 - 0915 UT. Average in situ temperature measurements at 600km are 4500 degrees K for the electrons and 2600 degrees K for the ions. Comparison between Figure 5a and 5b indicate the electron temperatures compare quite well. In situ ion temperatures show far more structure, and are roughly 500 degrees K higher than EISCAT values. It is important to recognize that altitude plots of the rocket data conflate horizontal motion, spatial structures, and temporal variations.

The 42 m radar shows evidence of NEIAL at altitudes 500 - 1000 km throughout the timeframe of the flight. The NEIALs were seen in 25 out of 72 data dumps taken by the 42 m between 0900 and 0915 UT (timeframe of SERSIO), and 39 out of 193 data dumps between 0850 and 0930 UT. The 32 m did not observe NEIAL. However, the 32 m reaches 500 km near the edge of the activity region shown in Figure 1. The 32 m is 18 degrees off the magnetic field, which is in excess of the typical angle off parallel NEIALs have been observed [*Collis et al*. 1991]. Thus, the absence of NEIAL in the 32 m is consistent with our expectations.

4.2 In situ data

Relevant in situ particle and wave data from 200-900 seconds TOF are summarized in Figure 6. Panel (a) shows energy spectra of the 5-16000 eV auroral electrons which clearly indicate the presence of a soft <1 keV population (Figure 3b). The 0.1-20 eV thermal ion spectra (panel (b)) indicate the payload charged to approximately -2 V, in agreement with a calculation based on *Fahleson* [1967] using the ERPA electron temperature data, even though the majority of the trajectory was in the sunlight. Thermal electron (panel (c)) and ion (panel (d)) temperatures were extracted from the ERPA and a HEEPS Thermal ion detector respectively. Panel (e) is a line plot of the square root of the integrated electric field power (25-5000 kHz). The final panel (f) shows the power spectrum for 0-20kHz waves obtained from the 1.8m baseline (spheres 3 and 4) of the COWBOY instrument.

Comparison between the panels at 350, 400, 500 seconds TOF reveals a strong correspondence between the thermal ion temperature enhancements and the BBELF (0-4kHz) wave activity. The wave power and ion temperature enhancements do not display a proportional relationship but clearly are collocated. At these times, the ion temperatures rise over 30% of the surrounding baseline values and the wave power below 4 kHz is increased by 1-3 orders of magnitude. The ACS malfunction caused the 1 and 2 sensors to be in contact, so we do not have density information from the HF wave data. Density calculated from the thermal ion data does not indicate the presence of any density holes associated with these ion temperature enhancements as seen in SCIFER rocket data [*Kintner et al.* 1996a]. However conclusive evidence of the existence of density cavities would require knowledge of the HF electric field and wave power at the plasma frequency.

It is interesting to note that the broad energy electron precipitation, which is generally observed to have a strong field aligned component, was generally coincident with periods of elevated thermal electron temperature (see panels a, c). The correspondence is clear on scales greater than 10 km. A relationship between the thermal electron and ion temperatures was not found, as they can either increase together (~500sTOF) or diverge (~400sTOF). Past ~550 s TOF or 9:06 UT, the payload exited the main auroral emission seen in the optical data, as shown by the decrease in the in situ data activity.

Figure 7 shows the VLF power spectrum inferred from the S3, S4, and 34 sensor pairs. The top panel shows power spectra relatively early in the flight when there was a brief burst of wave power across all frequencies; the lower panel shows a period of BBELF activity when there was less power above 10 kHz but power levels similar to the upper panel below 10 kHz. In the upper panel the wave power among the three baselines is virtually identical below 10 kHz while there is some differentiation above 10 kHz. In the lower panel the power levels between the three sensors are substantially different with the most power implied by the 3-4 sensor baseline (which is also the shortest baseline).

In general, different length baselines should all imply the same electric field power if the wavelengths are long (more than 2□*d, compared to the baseline). Hence when the S3 and S4 baselines imply smaller electric fields compared to the 34 baseline, the wavelengths must be less than roughly 30 m. Above the lower hybrid frequency (8 kHz

at 266 s and 6 kHz at 406 s), plasma waves often become short wavelength when auroral hiss propagates onto the lower hybrid resonance cone, which explains why the baselines imply different electric fields at higher frequencies. However the situation below 5 kHz is different. The top panel of Figure 7 shows that in the low altitude case the wavelengths are all long compared to the antenna baselines; the bottom panel shows that the wavelengths are short compared to 30 m at higher altitudes. The short wavelengths are consistent with three previous observations of BBELF wave activity within regions of perpendicular ion heating in the night side auroral oval [Bonnell et al, 1996; Kintner et al., 2000] and conclusively demonstrate that the waves associated with the ion heating are short wavelength BBELF.

5. DISCUSSION

This dual rocket/radar study of an ion upflow event provides the opportunity to compare two data sets and obtain a more complete altitude coverage of the ionosphere. In situ and radar thermal ion and electron temperatures are in general agreement for the timeframe of the flight. The in situ data (with much higher time resolution) recovers more structure above 500 km, especially in regions of wave heating. With enhanced electron density (Figure 2) and electron temperature (Figure 6) and the presence of auroral activity (Figure 1), we identify this as a type 2 ion upflow event [*Wahlund et al.* 1992]. We now consider the chain of processes that leads to this type 2 ion event, using our in situ and ground based observations to infer cause and effect.

5.1 NEIAL and BBELF

Wave activity seen in EISCAT data in the form of NEIAL has been attributed to mechanisms such as Langmuir turbulence and wave-wave decay [*Stromme et al*. 2004, *Forme and Fontaine* 1999]. NEIAL activity was seen throughout the time of the SERSIO observations. Scale sizes for ion acoustic wave regions are thought to be in the 100s of meter range, yet they can occur in multiple locations in a soft precipitation environment [Ogawa et al., Aspect angle dependence on NEIALs, to be submitted to Annales Geophysicae, 2006]. In situ and 42 m radar data are not in the same spatial location, yet they are in the same wide band of soft precipitation observed during the flight. While the rocket and 42 m radar were not collocated, they were studying the same region of activity as shown in Figure 1, so we can use SERSIO to look at the auroral electron energy distribution.

Figure 3b shows an example of the distribution at a time when the detector is roughly field aligned, and in a plasma environment with high thermal ion temperatures and strong BBELF wave activity. EISCAT 42 meter returns indicate a 6 s period of NEIAL around this time as well. The hot population seen throughout the flight is seen here as an unaccelerated Maxwellian with characteristic energy of about 200 eV. Lower energy, non-Maxwellian populations are seen below 100eV. This in situ electron distribution (typical of this event) is not one which would be expected to produce Langmuir turbulence, as it is very soft and does not include an accelerated inverted V “peak”, even a degraded one [*Ergun et al.* 1991]. Instead it is consistent with the soft precipitation commonly seen with BBELF activity [*Lynch et al.* 2002, *Bonnell et al*. 1996]. Thus the SERSIO/ESR observations indicate a link between NEIAL activity and BBELF.

The connection between ion upflows and NEIALs is well documented in the radar literature. Similarly, the connection between ion conics and BBELF is well documented in the in situ literature. Since SERSIO also shows a clear correspondence between regions of BBELF and ion heating in this region, we urge the NEIAL community to consider the possibility that BBELF and NEIAL are indicative of the same phenomena. *Wahlund et al.* [1993] linked increases in electron temperature with ion acoustic turbulence, as evidenced by NEIAL. Such an electron temperature increase raises the ratio of Te:Ti, which lowers the thresholds for current driven instabilities thought to be the driver for BBELF. In this manner, both BBELF and NEIAL can be linked to ion acoustic turbulence.

5.2 Wave activity and ion temperature

Figure 6 shows a clear local correspondence between soft precipitation enhancements and increased electron temperature, consistent with models showing soft precipitation to be the driver for ionospheric upflows [*Caton et al.* 1996 and *Su et al.* 1999]. Figure 6 also shows a clear correspondence between BBELF activity and elevated ion temperature. The connection between the electron enhancements (the driver) and the BBELF-ion temperature enhancements (the result) is a large scale one and not locally valid, as there can be holes in the precipitation when ion temperatures are elevated (see Figure 2, TOF~400 seconds). Let us consider first the BBELF-ion heating correspondence, and then the larger-scale picture.

Because of the ACS malfunction, efforts to attribute mechanisms to the multistage process of scale height increase and subsequent wave energization of ions to escape velocity are limited. Specifically, it is unfortunate that we do not have plasma flow information from the COWBOY instrument or our particle detectors. It is important to consider the possibility that our observed temperature enhancements could be caused by strong local unknown flows. To mimic a similar temperature increase as recorded by the thermal particle detector, the local ionosphere would need to support flows on the order of 2-3 km/s. The DMSP F13 satellite drift meter recorded flows on the order of 2 km/s when it crossed (0844-0847 UT) an extension of the same optical emission in which SERSIO flew [*Lorentzen et al.* 2006]. Even though local flows could mimic true temperature enhancements in the top hat detectors, we recognize the existence of BBELF where we see ion temperature enhancements. The nature of BBELF data acquired in previous flights, such as SCIFER [*Kintner et al*. 1996b], AMICIST [*Lynch et al.* 1996], and SIERRA [*Klatt et al*. 2005], support the idea that BBELF is a wave and not a Doppler shifted spatial structure. It is also of note that the relationship between wave power and ion temperature is not proportional as one would expect if they were both caused by rammed observation of spatial variations. The co-existence but non-proportionality of the wave power and the thermal ion enhancements indicates the relationship is not strictly local and depends on the time history of the flux tube. We therefore assume that our observed ion temperature enhancements are indicative of a true increase in ion temperature.

Similar to the SCIFER mission, we can associate this ion heating with BBELF activity. The fact that SCIFER covered 1400 km in altitude and SERSIO 782 km in altitude brings to light that these data show the BBELF interaction in the cusp/cleft at a lower altitude and much higher density than previously recorded. Nightside observations of transverse ion acceleration and BBELF waves were made by the AMICIST sounding rocket down to 500km, but this is the first observation at such low altitudes on the dayside where the density is much higher. [See Table 1 for a comparison of several rocket flights]. Modeling of this multistage ion heating process on the dayside should include wave heating effects at altitudes as least as low as 520 km and in densities well over 10^4 /cc.

Rocket	Apogee [km]	Density [1/cc]	Dayside/Nightside
SCIFER	1400	500-2000	Dayside
AMICIST	928	1000-5000	Nightside
SIERRA	735	20,000-60,000	Nightside
SERSIO	782	60,000-100,000	Dayside

Table 1. Comparison of four different sounding rocket missions and if ions are heated by BBELF wave activity.

It is interesting to note that even at these low altitudes, presumably near the origin of the ion upflow event, the ion temperature enhancements are not locally proportional to the simultaneous BBELF wave power. The BBELF measurements record the wave power at the instant of observation, while the ion temperature reflects the residence time of the ion population in the heating region. This nonproportionality is quite evident at FAST altitudes (4000 km) [*Lynch et al.* 2002], but is somewhat surprising so near the footpoint of the ion events. It indicates the variability of the BBELF-ion heating interaction.

These data then are consistent with the following picture. For this event, elevated electron temperatures seen in both the EISCAT data and the in situ detector can be interpreted as the response of the ambient thermal electrons to soft broad energy precipitation, as modeled by *Caton et al.* [1996] and *Su et al.* [1999]. This electron temperature enhancement creates an ambipolar field from electron scale height increase, which pulls the ions to higher altitudes. Subsequently, the ions enter a region where ion acoustic waves are unstable, producing BBELF and heating the thermal ions further towards escape velocity. Note that the enhanced electron temperature caused by the soft precipitation will also lower thresholds for current driven instabilities that can drive BBELF and NEIAL observations.

CONCLUSION

Our data indicate that wave induced ion heating can happen as low as 520 km in altitude and as high as 10^5 /cc in density in the dayside cusp/cleft. Wave activity seen as NEIAL in the radar was associated with BBELF in a nearby, though not collocated, auroral soft precipitation environment at the same time. The relationship between soft electron precipitation and thermal electron temperature enhancements recognized by the radar community is here also observed at finer spatial/temporal scales by the SERSIO experiment, with the soft precipitation seen as the original driver. The data from

sounding rocket flights in the cusp/cleft region are a critical element bridging the understanding gap between ground and satellite data. Future work will be focused on collaborations that can link these two research communities.

APPENDIX- ERPA analyzer

This new detector, a Faraday cup analyzer, uses a screen with a swept retarding potential (Figure 8). Electrons with energies less than the retarding potential are rejected and those with higher energies pass through the screen and are collected on an anode below. The current collected by the anode is measured by a low noise electrometer circuit.

The entrance face of the analyzer is held at a fixed +4 Volts relative to payload ground to accelerate electrons into the entrance in the presence of a negative payload potential. Gyroradius problems are minimized by keeping the analyzer dimensions small and mounting it in a field aligned direction. However, despite the fact that the ERPA was not aligned with the magnetic field on the SERSIO mission, it returned electron temperature data that matched EISCAT generated electron temperatures quite well (Figure 5).

ACKNOWLEDGEMENTS

The authors thank NASA Wallops Flight Facility, the NSROC team, the Andoya Rocket Range, and the Norwegian Coast Guard for their support of the SERSIO rocket flight. We recognize the engineering talents of Steve Powell, Dave Rau, Paul Vachon, Kevin Rhoads, Dave Collins, Ralph Gibson and Rob Michell. We also thank the EISCAT community and staff. We are also grateful for Richard Kaufmann's suggestions. This work was supported by NASA grant NAG5-5382 and NASA Space Grant NNG05GG76H.

REFERENCES

Arnoldy, R. L., K. A. Lynch, P. M. Kintner, J. Bonnell, T. E. Moore, and C. J. Pollock (1996), SCIFER- Structure of the cleft ion fountain at 1400 km altitude, *Geophys. Res. Lett*., *23*, 1869-1872.

Bonnell, J., P. Kintner, J.-E. Wahlund, K. Lynch, and R. Arnoldy (1996), Interferometric determination of broadband ELF wave phase velocity within a region of transverse auroral ion acceleration, *Geophys. Res. Lett., 23*, 3297-3300.

Canton, R., L. Horwitz, P. G. Richards, and C. Liu (1996), Modeling of F-region ionospheric upflows observed by EISCAT, *Geophys. Res. Lett., 23*, 1537-1540.

Carlson, C.W., D.W. Curtis, G. Paschmann and W. Michael (1983), An instrument for rapidly measuring plasma distribution functions with high resolution, *Adv. Sci. Res.,*, *2*, 67.

Collis, P. N., I. Haggstrom, K. Kaila, and M. T. Rietveld (1991), EISCAT radar observations of enhanced incoherent scatter spectra; their relation to red aurora and field-aligned currents, *Geophys. Res. Lett*., *18*, 1031–1034.

Ergun, R.E., C. W. Carlson, J. P. McFadden, J. H. Clemmons and M. H. Boehm (1991), Langmuir wave growth and electron bunching: results from a wave-particle correlator, *J. Geophys. Res.,* 96(A1), 225-238.

Fahleson, U. (1967), Theory of electric field measurements conducted in the magnetosphere with electric probes, *Space Sci. Rev.*, *7*, 238-262.

Forme, F. R. E., and D. Fontaine (1999), Enhanced ion acoustic fluctuations and ion outflows, *Ann. Geophys*., *17*, 182-189.

Forme F. R. E., D. Fontaine, and J. E. Wahlund (1995), Two different types of enhanced ion acoustic fluctuations observed in the upper atmosphere, *J. Geophys. Res., 100*, 14,625-14,636.

Grydeland, T., C. La Hoz, T. Hagfors, E. M. Blixt, S. Saito, A. Strømme, and A. Brekke (2003), Interferometric observations of filamentary structures associated with plasma instability in the auroral ionosphere, *Geophys. Res. Lett., 30*(6), 1338, doi:10.1029/2002GL016362.

Hultqvist, B., M. Øieroset, G. Paschmann and R. Trumann (Eds.) (1999), *Magnetospheric Plasma Sources and Losses*, Space Science Reviews, 88, Kluwer Academic Publishers, Dordrecht, The Netherlands.

Kintner, P. M., J. Bonnell, R. Arnoldy, K. Lynch, C. Pollock, T. Moore, J. Holtet, C. Deehr, H. Stenback-Nielson, R. Smith, and J. Olson (1996a), The SCIFER experiment, *Geophys. Res. Lett*., *23*, 1865-1868.

Kintner, P. M., J. Bonnell, R. Arnoldy, K. Lynch, C. Pollock, T. Moore (1996b), SCIFER – Transverse ion acceleration and plasma waves, *Geophys, Res. Lett*., *23*, 1873-1876.

Kintner P. M., J. Franz, P. Schuck, and E. Klatt (2000), Interferometric coherency determination of wavelength or What are BB-ELF waves?, *J. Geophys. Res., 105*(A9), 21, 237-21, 250.

Klatt, E. M., P. M. Kintner, C. E. Seyler, K. Liu, E. A. MacDonald, and K. A. Lynch (2005), SIERRA observations of Alfvenic processes in the topside auroral ionosphere, *J. Geophys. Res.*, *110*, A10S12, doi:10.1029/2004JA010883.

Lorentzen, D.A., P.A. Kintner, J. Moen, F. Sigernes, K. Oksavik, Y. Ogawa and J. Holmes (2006), Pulsating dayside aurora in relation to ion upflow events during a northward IMF dominated by a strongly negative IMF By. *J. Geophys. Res.,*

Lynch, K. A., R. L. Arnoldy, P. M. Kintner, P. Schuck, J. Bonnell, and V. Coffey (1999), Auroral ion acceleration from lower hybrid solitary structures: A summary of sounding rocket observations, *J. Geophys. Res., 104* (28), 515.

Lynch, K. A., J. W. Bonnell, C. W. Carlson, and W. J. Peria (2002), Return current region aurora: $\mathbf{E}_{par}$, $\mathbf{j}_z$, particle energization, and broadband ELF wave activity, *J. Geophys. Res.*, *107*(A7), 1115, doi:10.1029/2001JA900134.

Lynch, K. A., R. L. Arnoldy, P. M. Kintner, and J. Bonnell (1996), The AMICIST auroral sounding rocket: A comparison of transverse ion acceleration mechanisms, *Geophys. Res. Lett.*, *23*(23), 3293–3296.

MacDonald, E., K. Lynch, M. Widholm, R. Arnoldy, G. Lapenta, P. Kintner, E. Klatt (2005), In Situ Measurement of Thermal Electrons on the SIERRA Nightside Auroral Sounding Rocket, J. *Geophys. Res*., (revised).

Ogawa, Y., R. Fujii, S. C. Buchert, S. Nozawa, and S. Ohtani (2003), Simultaneous EISCAT Svalbard radar and DMSP observations of ion upflow in the dayside polar ionosphere, *J. Geophys. Res.*, *108*(A3), 1101.

Ogawa, Y., R. Fujii, S. C. Buchert, S. Nozawa, S. Watanabe, and A. P. van Eyken (2000), Simultaneous EISCAT Svalbard and VHF radar observations of ion upflows at different aspect angles, *Geophys. Res. Lett*., 27, 81-84.

Seo, Y., J. L. Horwitz, and R. Caton (1997), Statistical relationships between high-latitude ionospheric F region/topside upflows and their drivers: DE 2 observations, *J. Geophys, Res*., 102, 7493-7500.

Strangeway, R. J., R. E. Ergun, Y.-J. Su, C. W. Carlson, and R.C. Elphic (2005), Factors controlling ionospheric outflows observed at intermediate altitudes, *J. Geophys, Res*., 110, A03221.

Stromme, A., V. Belyey, T. Grydeland, C. La Hoz, U. P. Lovhaug, and B. Isham (2004), Evidence of naturally occurring wave-wave interactions in the polar ionosphere and its relation to naturally enhanced ion acoustic lines, *Geophys. Res. Lett*., 32, L05103.

Su, Y.-J., R. G. Caton, J. L. Horwitz, and P. G. Richards (1999), Systematic modeling of soft-electron precipitation effects on high-latitude F region and topside ionospheric upflows, *J. Geophys. Res.*, *104*, 153-163.

Wahlund, J. E., H. J. Opgenoorth, I. Haggstrom, K. J. Winser, and G. O. L. Jones (1992), EISCAT observations of topside ionospheric ion outflows during auroral activity: revisited*, J. Geophys. Res.*, 97, 3019-30337.

Wahlund, J. E., H. J. Opgenoorth, F. R. E. Forme, M. A. L. Persson, I. Haggstrom and J. Lilensten (1993), Electron energization in the topside auroral ionosphere: on the importance o f ion-acoustic turbulance, *J. Atm. Terr. Phys*., 55, 623-645.

Young, D. T., S. J. Bame, M. F. Thomsen, R. H. Martin, J. L. Burch, J. A. Marshall and B. Reinhard (1998), 2π-radian field-of-view toroidal electrostatic analyzer, *Rev. Sci Instrum.*, 59, 743.

Zheng, Y., T. E. Moore, F. S. Mozer, C. T. Russell, and J. Strangeway (2005), Polar study of ionospheric ion outflow verses energy input*, J. Geophys. Res*., 110, A07210.

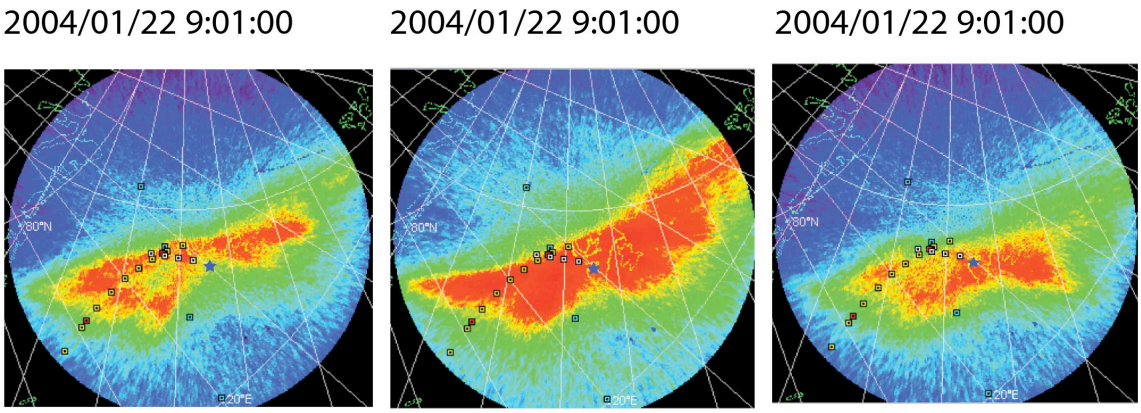

Figure 1. All sky images from Ny-Alesund UiO camera. 6300 Å emission projected to 250 km. SERSIO nominal trajectory shown in yellow.

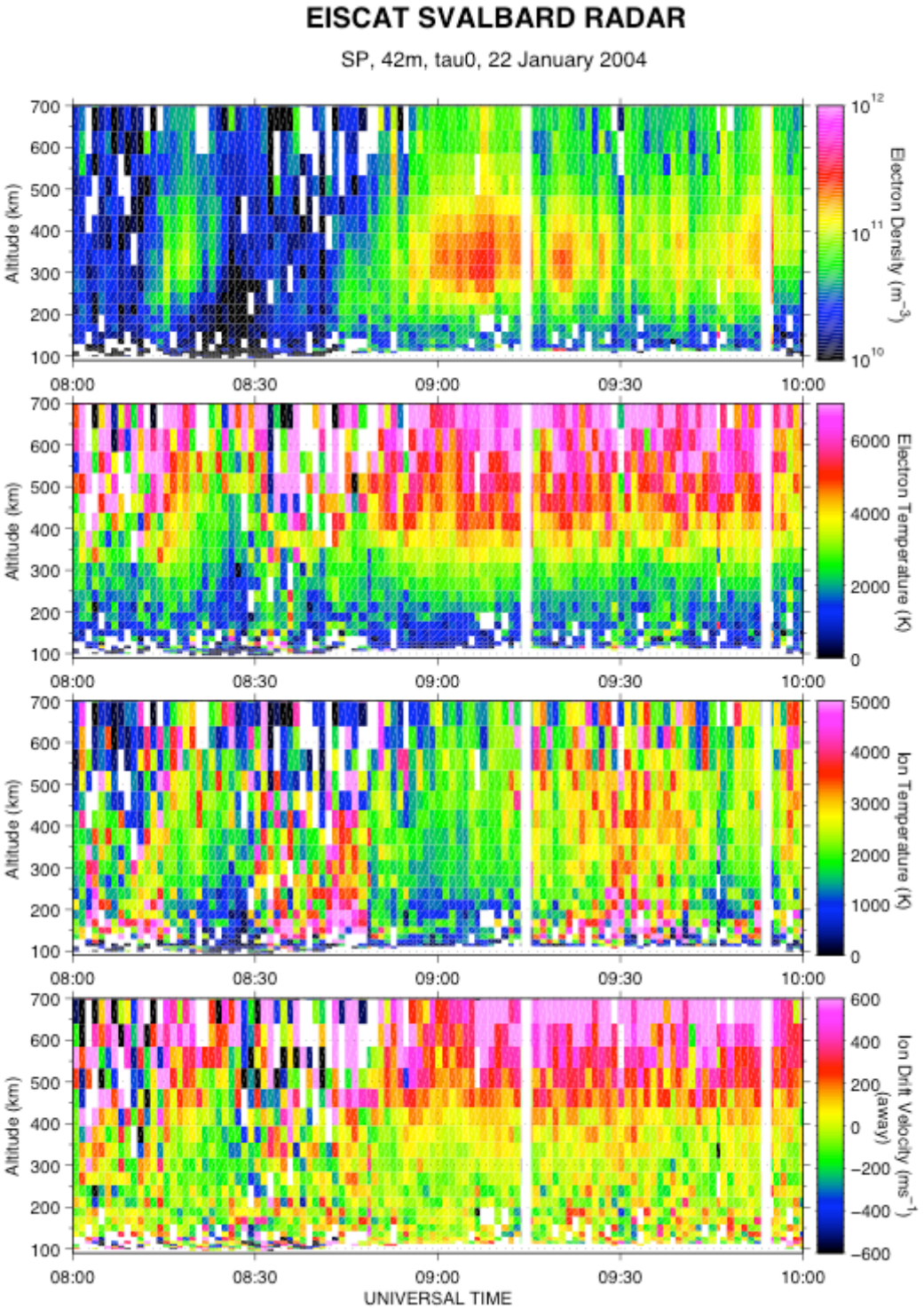

Figure 2. EISCAT spectra from 42m field-aligned antenna from Jan. 22, 2004

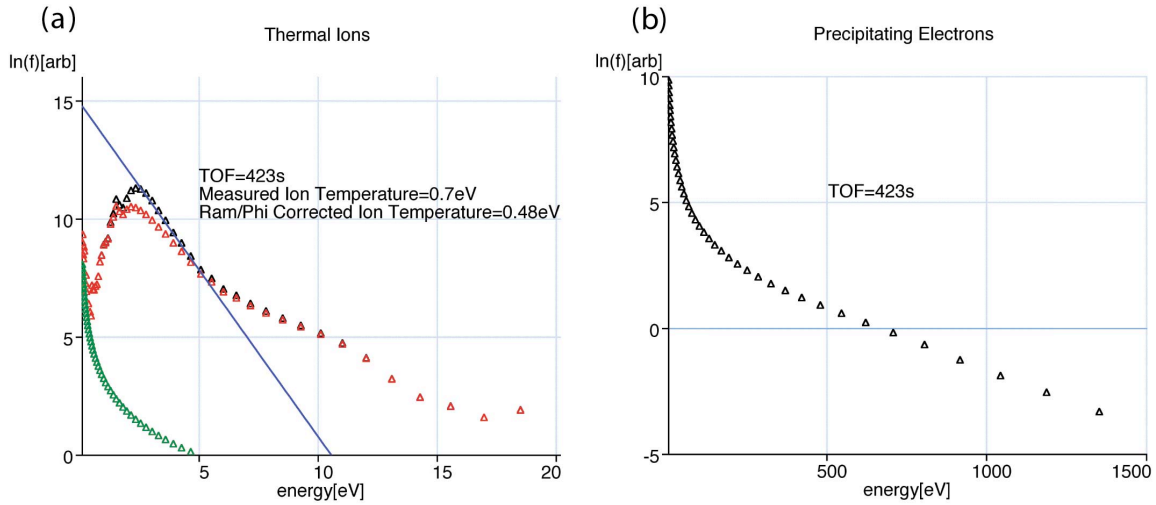

Figure 3. a) At 423 seconds TOF, this is a typical example of thermal ion distribution without dead-time correction (red) and with dead-time correction (black) and temperature fit (blue). The one-count level of the detector is shown in green. b) Example of precipitating electron distribution at 423 seconds TOF.

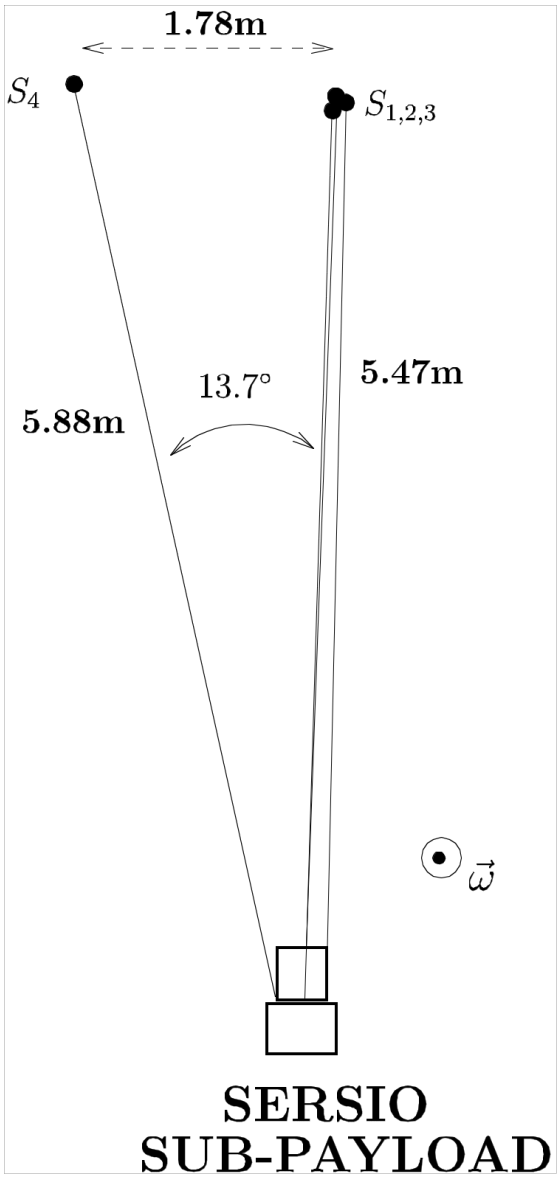

Figure 4. Cartoon of final configuration of COWBOY instrument.

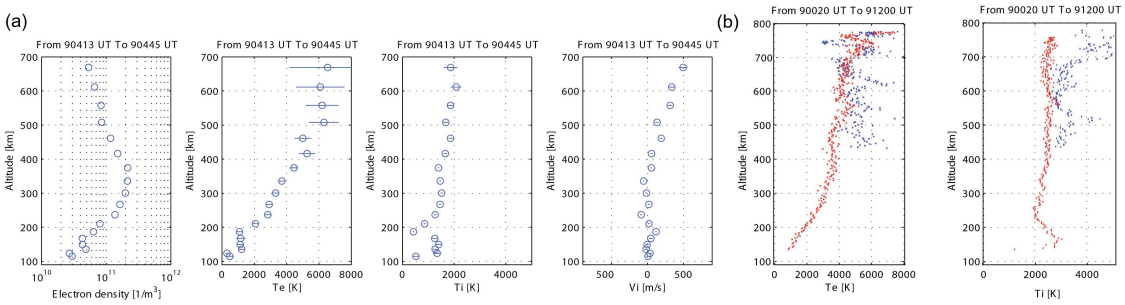

Figure 5. Altitude line plots from January 22, 2004 are presented from a) EISCAT, showing electron density, electron and ion temperatures, and ion velocity from the 42 meter field aligned dish 8:58:40 - 9:02:49 UT and b) in situ thermal electron and ion temperatures obtained from SERSIO flight 9:00:20 – 9:12:00 UT. Blue points differentiate the upleg from the red downleg points.

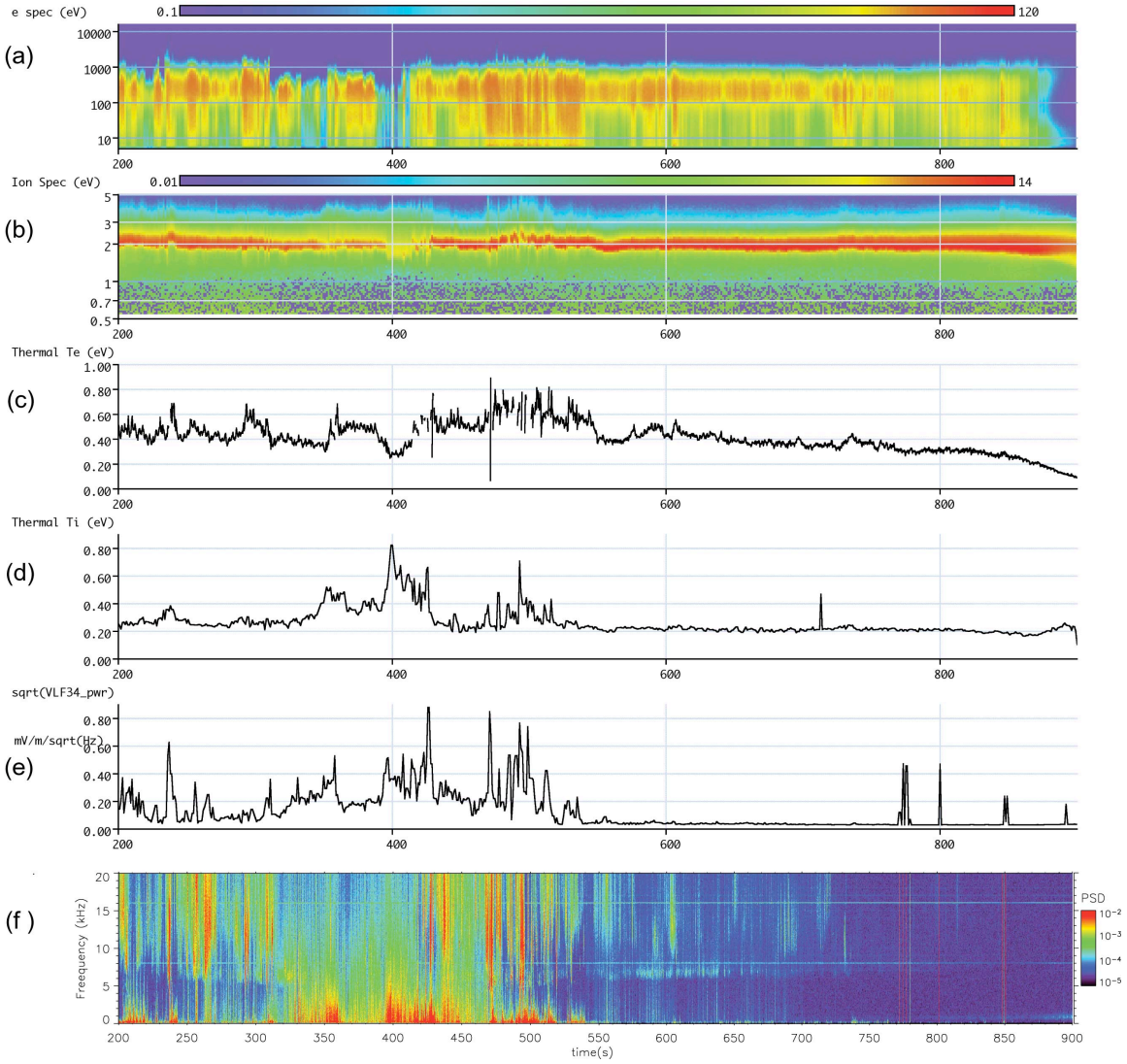

Figure 6. SERSIO a) precipitating electron spectrogram b) thermal ion spectrogram c) thermal electron temperatures extracted from the TED d) thermal ion temperatures corrected for ram effects e) square root of integrated electric field power (25-5000Hz) and f) wave power spectrum from the 1.8 m baseline of the COWBOY instrument plotted against time of flight in seconds.

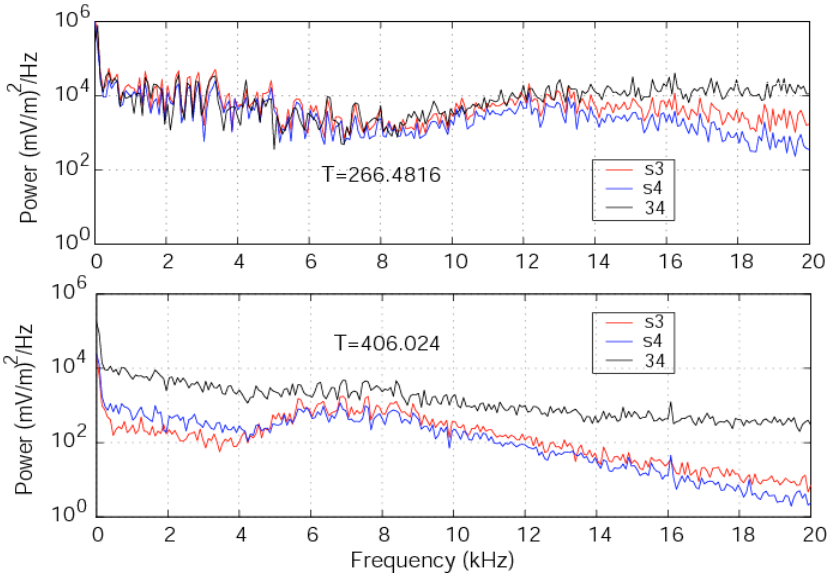

Figure 7. Comparison of the inferred electric field from three channels, skin to sensor 3, skin to sensor 4 and sensor 3 to sensor 4 with baselines of 5.5 m, 5.9 m, 1.8 m respectively. Note that the shortest baseline always implies that largest electric fields.

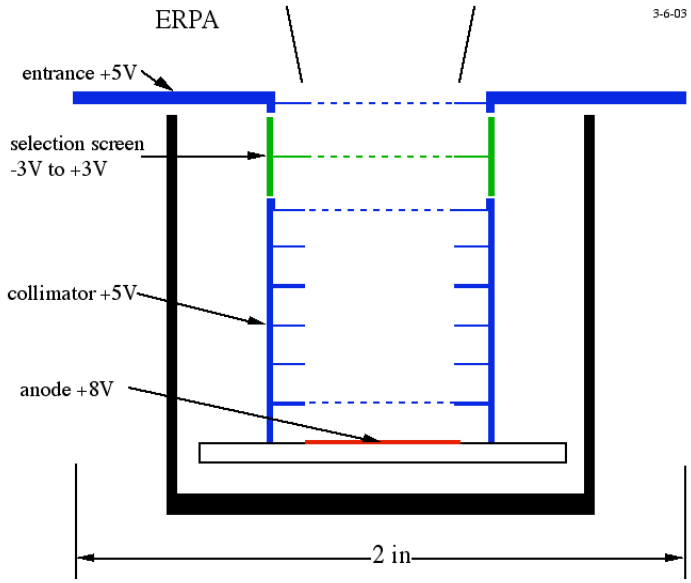

Figure 8. A schematic of the ERPA detector